Influence of the microstructure of two-dimensional random heterogeneous media on propagation of acoustic coherent waves

Adrien Rohfritsch, Jean-Marc Conoir, Tony Valier-Brasier, and Régis Marchiano
Sorbonne Université, CNRS, Institut Jean Le Rond ∂'Alembert, UMR 7190, 4 Place Jussieu, Paris, F-75005, France

(Received 3 December 2019; accepted 28 January 2020; published 12 February 2020)

Multiple scattering of waves arises in all fields of physics in either periodic or random media. For random media the organization of the microstructure (uniform or nonuniform statistical distribution of scatterers) has effects on the propagation of coherent waves. Using a recent exact resolution method and different homogenization theories, the effects of the microstructure on the effective wave number are investigated over a large frequency range (ka between 0.1 and 13.4) and high concentrations. For uniform random media, increasing the configurational constraint makes the media more transparent for low frequencies and less for high frequencies. As a side but important result, we show that two of the homogenization models considered here appear to be very efficient at high frequency up to a concentration of 60% in the case of uniform media. For nonuniform media, for which clustered and periodic aggregates appear, the main effect is to reduce the magnitude of resonances and to make network effects appear. In this case, homogenization theories are not relevant to make a detailed analysis.

DOI: 10.1103/PhysRevE.101.023001

I. INTRODUCTION

For more than a century, authors in theoretical physics and applied mathematics have proposed numerous models for studying multiple scattering and propagation of waves in random inhomogeneous media. Multiple scattering in random media is of practical interest in many fields of physics ranging from the theory of randomly disordered crystals [1], the resonant scattering of light [2], the ultrasonic monitoring of colloidal mixtures [3], the effective dynamic mass density of composites [4] the propagation of waves in trabecular bones [5], metamaterials [6], the scattering from clusters of bubbles [7], and the propagation through high-density hyperuniform materials [8], to name a few. Reviews of the best-known models and their mathematical backgrounds can be found in Refs. [9–14]. Broadly speaking, there are three different types of models: (1) those based on Green functions and diagrammatic techniques like Feynman diagrams [11,13], which has led to independent scattering approximation (ISA) and coherent potential approximation (CPA) [12]; (2) those coming from the multiple scattering equations initiated by Foldy [15] and Lax [16], with the most famous formula based on the Lax quasicrystalline approximation probably that of Waterman and Truell (WT) [17]; and (3) the models where the ensemble-averaged equations are calculated from the local constitutive equations of the continuous and dispersed phases using a configurational average [18–20].

Among all these models, one can distinguish those that give an analytical expression of the effective wave number describing the propagation in the multiple scattering medium, such as ISA and WT, from the self-consistent models where the effective wave number is obtained by searching for the root of characteristic equations, as with the CPA and the generalized self-consistent model (GSCM) developed by Yang and Mal [21]. There are some relationships between models. For example, ISA and WT are comparable when the backscattering of particles is negligible compared to the forward scattering, and the GSCM was derived using an iterative self-consistent scheme applied to the WT formula. This scheme can also be applied to any analytical expressions of the effective wave number, such as the Linton and Martin (LM) formula [22], to get a new self-consistent model [23]. Finally, to be complete, if we also take into account models based on other approaches, like those of Refs. [24–29], we end up with a very large number of solutions for calculating effective wave numbers, and the question is: What is the best one? Not surprisingly, the answer to this question depends on the context in which it raised. A comparative study was recently carried out between eight models for shear waves [28]. It is a challenging and difficult task because at least three parameters have to be taken into account: the concentration of particles, the frequency, and the type of particles; some of them can be very resonant as bubbles [7], and others are "weak scatterers" as aggregates contained in a cement matrix (concrete) [30]. Disagreements between models obviously increase with the concentration of particles, but not exclusively [28]. To conclude this brief overview, we refer here to the analysis of Kim about discrepancies observed between numerical results [28]: "Therefore, a blind comparison between experimental and theoretical results ignoring the composite's micro-structure can lead to a meaningless conclusion." In the following, reacting to this analysis, the role played by the microstructure of random media in the propagation of coherent waves is investigated.

II. FRAMEWORK OF THE STUDY

Facing the difficulty of analyzing a wide variety of random media apart from the research context, as outlined above,

it is necessary to establish a precise framework so as to limit the study field and focus on the role played by microstructures. By microstructure, we mean the configurational organization of the scatterers in a homogeneous matrix. We distinguish two categories of random media: the uniform random media whose statistical properties are uniform and nonuniform random media whose statistical properties are not. Of course, other parameters can play an important role on the propagation of coherent waves: the type of particles, the concentration, the polydispersity associated to the different size of particles, and the anisotropy. The polydispersity is known to enlarge the width of resonances and to reduce their influence. This well-known effect will not be considered here as well as the anisotropy related to the shape of particles.

Though the basic physical concepts in multiple wave scattering can be applied to whatever types of wave, acoustics is known to be a convenient framework to study multiple scattering mainly because of the versatility of the experimental measurements, which provide access to the instantaneous pressure (with the phase) and not only the intensity of the waves. For instance, Derode *et al.* [31] studied experimentally the influence of correlations between scatterers using a random collection of parallel steel rods immersed in water. In order to have comparisons with experiments for some configurations, we have chosen to investigate the same kind of random media. Furthermore, this kind of heterogeneous medium is very interesting to study because steel rods are strongly resonant as are spherical scatterers, the so-called Mie particles in optics [2]. For this study, we will use in-house software, called MuScat, which is able to address this problem with several tens of thousand scatterers, for any kind of geometry [32]. That allows us to model any microstructure in detail without approximation except the inherent numerical errors.

This work is organized as follows. Section III contains the processes to build the different random media considered in this paper. Section IV gives a brief overview of the numerical software MuScat and explains the choice of the two homogenization methods which have been selected among many others. Section V deals with uniform random media. First, numerical results obtained at low concentration by the homogenization models and the numerical software are compared to experimental data from Derode *et al.* [31]. Then the impact of the microstructure at higher concentration is studied at large and small wavelengths, respectively. Finally, the effects of the microstructure of nonuniform random media are investigated in Sec. VI.

III. DESIGN OF THE MICROSTRUCTURES

A. Construction of the uniform random media

The uniform random media are built following the experimental procedure set up by Derode *et al.* [31]. A slab of surface S contains n_0 identical scatterers, so the concentration is $\phi = n_0\pi a^2/S$. Their positions are computed using a random draw considering an exclusion distance b between two scatterers in order to avoid their overlapping. Experimentally, the exclusion distance is fixed by the fact that steel rods are hold by two plates, from top and bottom, in which holes have been drilled. The exclusion distance is then regarded as the minimum distance between a pair of holes (with origin at the center of the holes).

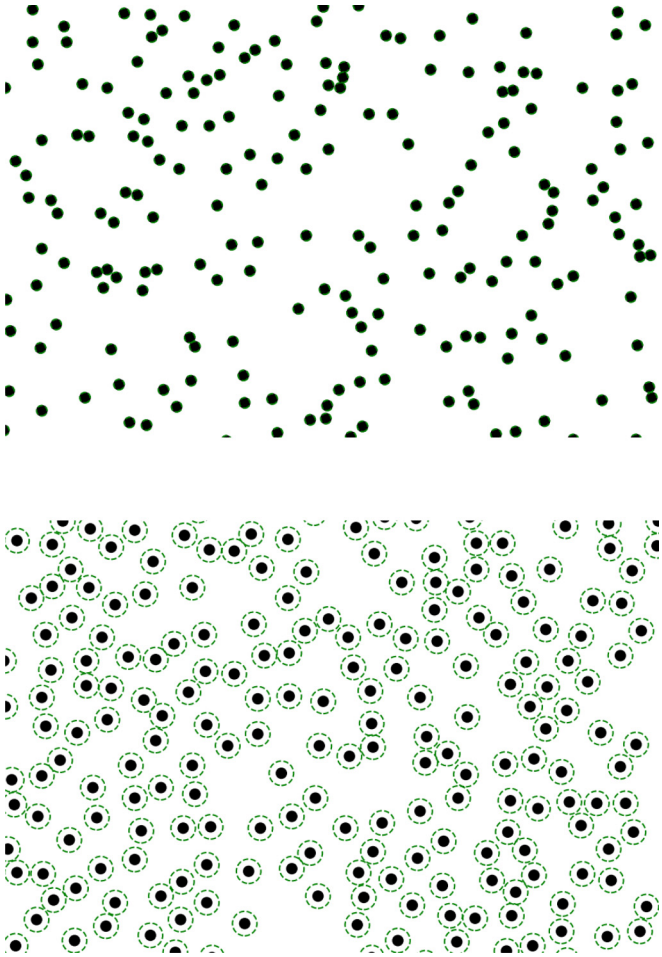

FIG. 1. Two random microstructures with concentration $\phi = 6\%$, with $b \to 2a$ (top) and $b = 4.82a$ (bottom). The exclusion distance b is the minimum distance between the centers of a pair of scatterers. Dotted green circles have a radius of $b/2$.

Before going further, let us look at what can be said concerning the exclusion distance b and its impact on the microstructure of the multiple scattering media. Figure 1 shows two distributions with concentration $\phi = 6\%$ constructed for two values of b. For the first distribution (up), $b \to 2a$, which allows two particles to be infinitely close, without being in contact. This value is the smallest one for the exclusion distance without interpenetration. For the second distribution (bottom), we use the value $b = 4.82a$ imposed in the experiments by Derode *et al.* [31]. As noted by Conley *et al.* [33], it is obvious that increasing b decreases the positional "freedom" of the cylinders. So we can say that the exclusion distance b has an influence on the microstructure. Noting $\phi_b = n_0\pi(b/2)^2/S$, one has

$$\frac{\phi_b}{\phi} = \frac{b^2}{4a^2}. \tag{1}$$

Keeping in mind that the most concentrated medium cannot have a concentration higher than $\phi_{\max} = \pi/2\sqrt{3} \approx 0.907$ (for

TABLE I. Values of $b/2a = \sqrt{0.35/\phi}$ and $b_{\max}$ corresponding to different concentrations ϕ.

ϕ (%)	$b_{\max}/2a$	$b/2a = \sqrt{0.35/\phi}$
6	3.89	2.41
14	2.54	1.58
30	1.74	1.08

monodisperse medium in two dimensions), $\phi_b \leqslant \phi_{\max}$ implies

$$b_{\max} = 2a\sqrt{\frac{\pi}{2\sqrt{3}\phi}} \approx 2a\sqrt{\frac{0.907}{\phi}}. \quad (2)$$

The main information contained in Eq. (2) is the proportionality of $b_{\max}$ with $1/\sqrt{\phi}$. In this work, we investigate the propagation through media with varying concentrations. In addition to imposing $b < b_{\max}$, the microstructure is constrained in the same manner whatever the value of the concentration, by imposing

$$b = 2a\sqrt{\frac{0.35}{\phi}}. \quad (3)$$

The relation of Eq. (3) is the same than the one chosen by Derode *et al.* [31]. The values of b used in the numerical simulations are given in Table I for few values of concentration ϕ. Unless otherwise stated, we chose to set the value of b in the same way for all the results presented in this paper.

Paraphrasing Conley *et al.* [33], we can say that the short-range correlation in the disorder is controlled by imposing a minimum distance b between the centers of two cylinders. The idea is that b is not only a parameter related to the geometry (microstructure) but also a parameter that allows us to characterize the effect of the correlation on the propagation of waves. In short, the idea developed in the following is that microstructures are characterized by two parameters, the concentration ϕ and the degree of correlation b. Propagation through this type of media is discussed in Sec. IV B.

B. Construction of the nonuniform random media

In this section, two types of microstructure that are not statistically uniform are considered. Both can be built using the random walk process presented in the work of Mallet *et al.* [34]. Starting from a given position in the space, knowing the borders of the medium and the concentration desired, we perform random walks with a given step length and orientation selected at random between N_θ possibilities. At each step (of constant length), an orientation θ is selected between $-\pi$ and π. Either the new position is free, in this case a scatterer is placed, or the position is occupied, in which case another position is selected at random and the walk starts again.

The first microstructure is constructed following this process, with $N_\theta = 1000$ possible orientations selected at random. When the step of the walk is small enough, this procedure leads to a clustering effect, as shown in Fig. 2(a), which is constructed with a step of 2.2a. Clustering is a consequence of the fact this procedure always induces a return to the point of departure. As illustrated by this example, such a medium is characterized by very strong variations of local concentration (clustering).

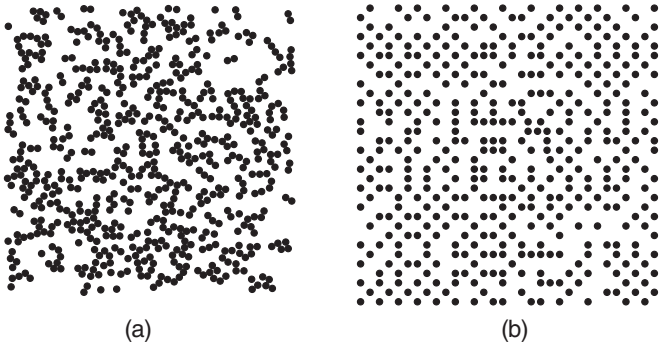

FIG. 2. Examples of nonuniform random microstructures constructed by random walk process. Panel (a) is constructed with $N_\theta = 1000$; panel (b) is constructed with $N_\theta = 4$ and crystal-like geometrical properties with cell length d.

The second type of microstructure is also built with this procedure, but with $N_\theta = 4$, so that the orientation can be assimilated to the cardinal points. This choice leads to building a crystal with defects but with periodic cells into the microstructure. According to the points of view, the medium can be considered as a crystal with random defects, but also as a collection of small clusters, each of them containing a few periodically spaced cylinders. An example of such medium is shown in Fig. 2(b) where the medium is composed of randomly distributed scatterers on the nodes of a periodic lattice of characteristic length d. Propagation through these types of media is discussed in Sec. VI.

IV. CALCULATION METHODS OF THE EFFECTIVE PARAMETERS

A. Semianalytical method: MuScat

A large overview of numerical methods applied to multiple scattering has been presented recently by Amirkulova and Norris [35], and more details can be obtained by referring to Refs. [36,37] and to the books written by Martin [14] and Gumerov and Duraiswami [38], the latter presenting an up-to-date discussion about the fast multipole method (FMM). In a recent work, the exact formulation of multiple scattering problem is presented. This formulation allows the computation of the modal scattering amplitudes of N_s infinite cylinders immersed in a fluid host medium. For numerous scatterers and high frequencies, this resolution is challenging but has been done recently with the in-house software MuScat [32].

The general idea is to decompose the acoustic field as the sum of the incident field and all the waves scattered by the cylinders. The harmonic field p can be decomposed into the basis of the cylindrical harmonics (for simplicity the time dependency $e^{-i\omega t}$ is omitted below). Considering a distribution of N_s cylinders arbitrarily distributed and of arbitrary acoustical properties, the total field is

expressed as

$$p(\mathbf{r}) = p_{\text{inc}}(\mathbf{r}) + \sum_{j=1}^{N_s} p_s^{(j)}(\mathbf{r_j}), \tag{4}$$

with $p_{\text{inc}}(\mathbf{r})$ the incident wave and $p_s^{(j)}(\mathbf{r_j})$ the wave scattered by the jth cylinder expressed with respect to coordinates $\mathbf{r} = (r, \theta)$ and $\mathbf{r_j} = (r_j, \theta_j)$. They are given in term of modal sums by

$$\begin{cases} p_{\text{inc}}(\mathbf{r}) = \sum_{n=-\infty}^{+\infty} d_n J_n(kr) e^{in\theta}, \\ p_s^{(j)}(\mathbf{r_j}) = \sum_{n=-\infty}^{+\infty} A_n^{(j)} H_n^{(1)}(kr_j) e^{in\theta_j}, \end{cases} \tag{5}$$

where k is the wave number, coefficients d_n are the amplitudes of each mode of vibration ($d_n = i^n$ for a plane wave), J_n is the Bessel function of order n, and $H_n^{(1)}$ is the Hankel function of the first kind of order n. The linear block system satisfied by the coefficients $A_n^{(j)}$ can be formulated in a matricial way as

$$[\mathcal{I} - \mathcal{T}\mathcal{M}]\mathbf{A} = \mathcal{T}\mathbf{E}, \tag{6}$$

with $\mathcal{T}$ the block matrix containing all the $\mathbb{T}^{(j)}$ matrix collecting the scattering coefficients of every scatterer j and the following notations:

$$\begin{cases} \mathbf{A} = (\mathbf{A}^{(1)}, \mathbf{A}^{(2)}, \ldots, \mathbf{A}^{(N_s)})^t, \\ \mathbf{E}_p = \mathbb{N}^{(0p)}\mathbf{d}, \\ \mathcal{T}_{pq} = \mathbb{T}^{(p)}\delta_{pq}, \\ \mathcal{M}_{pq} = \mathbb{M}^{(pq)}(1 - \delta_{pq}), \end{cases} \tag{7}$$

and the matrices coefficients

$$\begin{cases} M_{\nu n}^{(kj)} = H_{\nu-n}^{(1)}(kr_{kj}) e^{i(\nu-n)\theta_{kj}}, \\ N_{\nu n}^{(0j)} = J_{\nu-n}(kr_{0j}) e^{i(\nu-n)\theta_{0j}}. \end{cases} \tag{8}$$

The resolution of the system (6) gives the exact amplitudes of scattering waves by each scatterer. In MuScat the possibility of neglecting the long-distance interactions between cylinders has been precisely discussed. In this work, as far as the media considered are relatively small, all the interactions have been taken into account. The acoustic pressure is calculated at the end of a slab of width h in the direction of propagation containing or not a random set of parallel cylinders:

$$\begin{cases} p_0 = Ae^{ikh} & \text{in homogeneous medium,} \\ p_1 = Ae^{ik_{\text{eff}}h} & \text{in heterogeneous medium,} \end{cases} \tag{9}$$

where the effective wave number is noted $k_{\text{eff}} = \omega/c_{\text{eff}} + i\alpha_{\text{eff}}$, with c_{eff} the effective phase velocity and α_{eff} the effective attenuation. These effective parameters are all calculated due to an average process on several tens of distributions and are given by

$$\begin{cases} \alpha_{\text{eff}} = -\frac{1}{h} \ln\left(\left|\frac{p_1}{p_0}\right|\right), \\ c_{\text{eff}} = \frac{\omega h}{\frac{\omega h}{c_0} + \arg\left(\frac{p_1}{p_0}\right)}. \end{cases} \tag{10}$$

B. Homogenization models

Among the many homogenization models, we chose two models that contain explicitly a parameter similar to the exclusion distance b. The first model is the one presented by Derode *et al.* and named "Keller" for reasons explained in Ref. [31]. Its main interest lies in the fact that the correlation is explicitly taken into account by introducing the Percus-Yevick approximation (PYa). It follows that this model results in a clear analysis in terms of correlation, analysis based on Green functions, and diagrammatic representations of the multiple scattering, which forms the main interest of this approach. With this model, the effective wave number k_{Kell} is given by

$$k_{\text{Kell}}^2 = k_{\text{ISA}}^2 - \left(4in_0 \sum_{n=-\infty}^{+\infty} T_n\right)^2 \times \int_0^\infty \frac{i\pi}{2} H_0^{(1)}(kr) J_0(kr)[1 - g(r)] r\, dr, \tag{11}$$

where T_n is the scattering coefficient of order n associated with each cylinder. In Eq. (11) the first term k_{ISA} corresponds to the ISA given by

$$k_{\text{ISA}}^2 = k^2 - 4in_0 \sum_{n=-\infty}^{+\infty} T_n \tag{12}$$

and the second term to the PYa. Note here that the PYa includes only the component corresponding to the mode of vibration $n = 0$, the others being neglected. The function $g(r)$ is calculated such that $n_0 g(r)$ gives the concentration at a distance r from the center of a scatterer. Here $g(r)$ is computed from numerical simulations of random distributions as in Ref. [31].

The second model was initially derived by Fikioris and Waterman (FW) [39]. In this model, the parameter b is fixed to the value $b = 2a$ corresponding to the hole correction (HC) for which $g(r) = 0$ when $r < 2a$ and $g(r) = 1$ otherwise. Compared to ISA, the FW model introduces a second-order term in concentration as

$$k_{\text{FW}}^2 = k_{\text{ISA}}^2 + d_2 n_0^2, \tag{13}$$

with, noting $p = |m - n|$,

$$d_2 = \frac{4i}{\pi k^2} \sum_{n=-\infty}^{+\infty} \sum_{m=-\infty}^{+\infty} \left[(k^2b^2 - p^2) J_p(kb) H_p^{(1)}(kb) + k^2 b^2 J_p'(kb) H_p'^{(1)}(kb)\right] T_n T_m. \tag{14}$$

Here we would like to digress briefly about the reason why the parameter b was introduced. The FW model leads us to calculate divergent integrals for the modes $n \geqslant 2$. This is the mathematical reason why singularities are surrounded by a cylinder of radius b to avoid the divergence of the integrals. From a mathematical point of view, b can take any value, but it is not satisfying from a physical point of view to introduce a parameter without physical interpretation. One can assume that this is the reason for which different values of b are imposed in the literature to circumvent this "lack of meaning." The HC leads to set $b = 2a$, which is essentially a nonoverlapping condition between scatterers. Using $b \to 0$

leads to the LM model [22]

$$k_{\mathrm{LM}} = \lim_{b\to 0} k_{\mathrm{FW}}. \tag{15}$$

The expression (15) clearly shows that LM model does not take correlation into account, since $b \to 0$, but is still a second-order model in concentration. The ISA wave number, which is the first term of every other model, will be shown as well. It is adapted to point scattering, which corresponds to the case when the wavelength of the incident wave is much larger than the characteristic length scale of the scatterers [40]. In this context, among the models that go beyond "ISA," some of them are not only based on the Dyson equation, as in our case, but go further by considering the Bethe-Salpeter equation that gives access to the correlation, thereby including all induced dipole-dipole interactions [41]. We are then in the field of transport theories, which are out of the scope of our study.

As mentioned before, assuming a modified form of the HC with hole radius b and oscillations depending on the concentration leads to the PYa [42]. However, nothing prevents us from giving to b the value we want provided that b has a physical meaning. This is the reason the value of b chosen is the same as the one introduced in the experimental setup as well as in MuScat simulations. The important point to emphasize here is that FW and Muscat, contrary to Keller, do not introduce the PYa to model the correlation.

To conclude, let us state that comparison between LM and ISA on the one hand and FW and Keller on the other hand can therefore be useful to distinguish concentration effects from correlation effects. Removing the correlation from the Keller model leads to ISA, whereas removing correlation in the FW model leads to the LM model.

V. PROPAGATION IN UNIFORM RANDOM MEDIA

A. Comparison of models with experiments: Link between exclusion distance b and degree of correlation

We consider the propagation of coherent waves through a cluster of parallel steel rods immersed in water. Scatterer radii are $a = 0.4\,\mathrm{mm}$, and the acoustical properties $c_L = 5700\,\mathrm{m/s}$, $c_T = 3000\,\mathrm{m/s}$, and $\rho_c = 7850\,\mathrm{kg/m^3}$. Speed of sound in water is taken as $c_0 = 1500\,\mathrm{m/s}$ and density as $\rho_0 = 1000\mathrm{kg/m^3}$. With MuScat, the coherent wave is obtained by averaging until convergence (between 30 and 50 draws).

Two experimental data sets are presented here, taken from Derode *et al.* [31], one with a concentration $\phi = 6\%$ and the second one with $\phi = 14\%$. The frequency range experimentally explored is 2–4 MHz, which corresponds to parameter ka included in 3.35–6.7. Such a high-frequency range imposes to take into account the nine first modes in MuScat to correctly measure the effective parameters, even if the resonances come from modes 1 and 2. The quantity presented here is the elastic mean-free path l_e, directly linked to the effective attenuation α_{eff} by the relation

$$l_e = \frac{1}{2\alpha_{\mathrm{eff}}}. \tag{16}$$

For both concentrations, MuScat and experimental results are also compared to ISA, FW, and Keller. In Figs. 3(a) and 4(a), the value of b used in numerical results is set to $2a$,

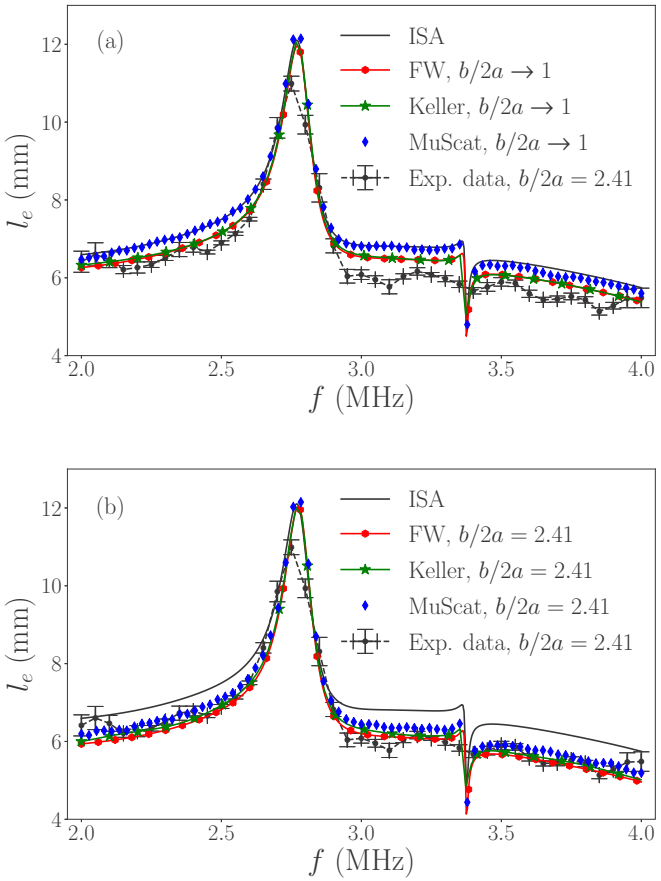

FIG. 3. Scattering mean-free path of a slab with density $\phi = 6\%$, and $b/2a \to 1$ (a) or $b/2a = 2.41$ (b): comparison between experimental results, MuScat simulations, and homogenization calculations. Frequency range corresponds to $ka \in [3.35 - 6.7]$.

and that is set to values given in Table I in Figs. 3(b) and 4(b). Changing b in the FW model affects the mean-free path [given by Eq. (16)] in the same way as in MuScat simulations. In addition, the Keller and FW models give very similar results which are both in good agreement with experiments. These last results support the idea that the parameter b is not only an exclusion distance but can also be considered as a degree of correlation characterizing the microstructure and the propagation of coherent waves. This is the principal result of this section apart from the fact that there is a very good agreement between MuScat and homogenization models. The next section is devoted to investigating propagation in much more concentrated uniform media up to 60% in concentration for a larger frequency range.

B. Correlation effects at high frequency

The aim of this part is to study the influence of the correlation on the wave propagation in high concentrated media. Another objective is also to determine the extent to which the homogenization and statistical models are appropriate in order to estimate correctly the effective wave numbers at high frequency. To be complete, we will also show predictions from LM and ISA models.

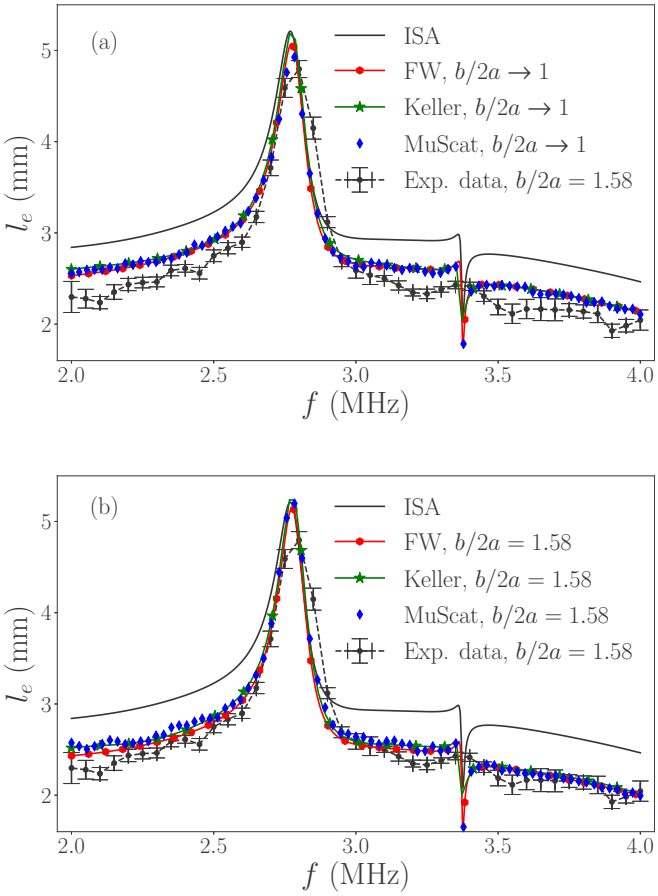

FIG. 4. Scattering mean-free path of a slab with concentration $\phi = 14\%$, and $b/2a \to 1$ (a) or $b/2a = 1.58$ (b): comparison between experimental results, MuScat simulations, and homogenization calculations. Frequency range corresponds to $ka \in [3.35 - 6.7]$.

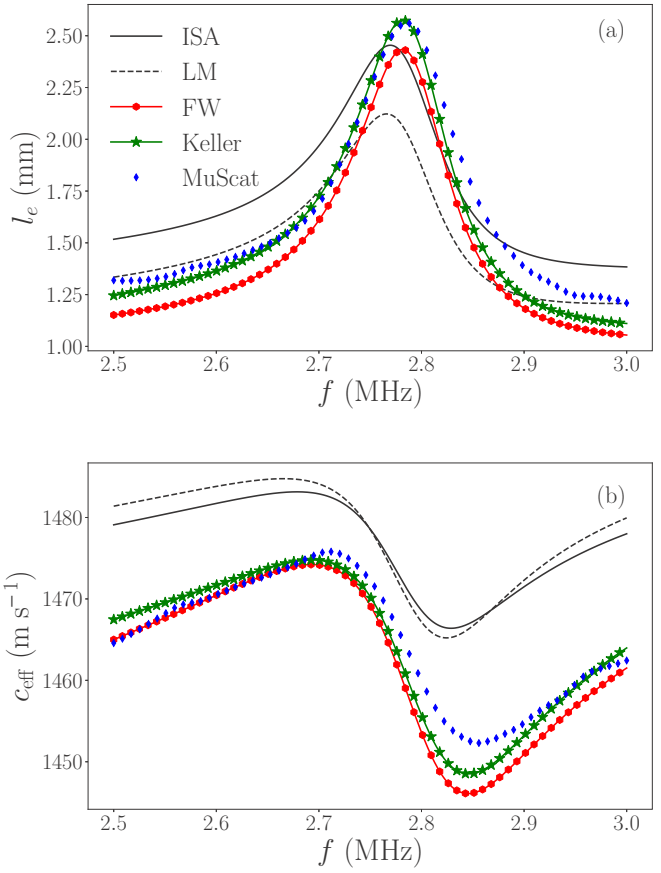

FIG. 5. Effective attenuation (a) and effective phase velocity (b) for a concentration of $\phi = 30\%$, calculated with MuScat (diamonds markers) and different statistic models: Linton and Martin (LM), Fikioris and Waterman (FW), ISA, and Keller. Frequency range corresponds to $ka \in [4.18–5.02]$.

As mentioned in Sec. III B, the exclusion distance b given by relation (3) allows us to build distributions for $b > 2a$ with concentration up to $\phi = 35\%$. In the following the most concentrated medium which is investigated has a concentration $\phi = 60\%$. To ensure $b > 2a$ in this extreme case, the relation

$$b = 2a\sqrt{\frac{0.65}{\phi}} \tag{17}$$

is set to link b and ϕ in agreement with the values given in Table II.

We start by focusing on what is happening around the resonance frequency $f = 2.77$ MHz (observed in Figs. 3 and 4) for an intermediate concentration which is set at $\phi = 30\%$. Figure 5 shows the predictions of l_e and c_{eff} of all models around this resonance frequency. The first phenomenon that is noticeable is that FW and Keller as well as MuScat models predict that the multiple scattering has a strong impact on the position of the resonance frequency, which is shifted towards high frequencies, even if the concentration is not so large. Of course, this effect increases with the concentration, which is why it is less visible in Figs. 3 and 4. This phenomenon appears only in models that take the correlation into account, suggesting that the resonance shift is closely linked to the microstructure and cannot be explained by a simple effect of multiple scattering neglecting the correlation.

Let us now look at the behavior of the resonance frequency with regard to the concentration. To this end, the degree of correlation b is assumed to depend on the concentration according to the relation Eq. (17) in order to keep a medium under the same configurational constraint. Figure 6 shows the attenuation [Fig. 6(a)], inversely proportional to the elastic mean-free path, and the phase velocity [Fig. 6(b)] as functions of concentration. Comparing ISA and LM to Keller, FW, and MuScat, we see that the correlation clearly drives the attenuation down (the scattering mean-free path up). This behavior is the opposite of what happens outside the resonance, as shown in Fig. 6(c) at the frequency $f = 4.0$ MHz. Concerning the resonance frequency, it is remarkable that ISA gives good

TABLE II. Values of $b = 2a\sqrt{0.65/\phi}$ and $b_{\max}$ corresponding to different concentrations ϕ.

$\phi(\%)$	$b_{\max}/2a$	$b/2a = \sqrt{0.65/\phi}$
6	3.89	3.29
14	2.54	2.15
30	1.75	1.47

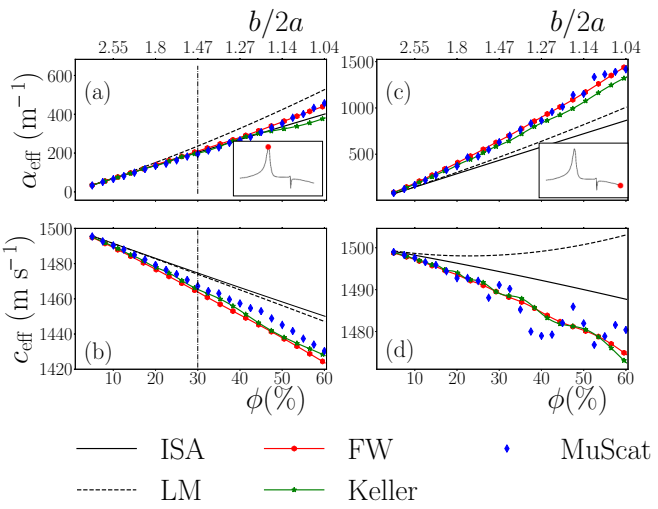

FIG. 6. Effective attenuation and phase velocity as a function of the concentration, for frequency $f = 2.77$ MHz, $ka = 4.64$ [(a) and (b)], which corresponds to a resonance frequency, and $f = 4$ MHz, $ka = 6.7$ [(c) and (d)]. The dots on the subplots show the relative position on the spectrum of Figs. 3 and 4. The vertical dotted line corresponds to the concentration chosen to calculate effective parameters of Fig. 5.

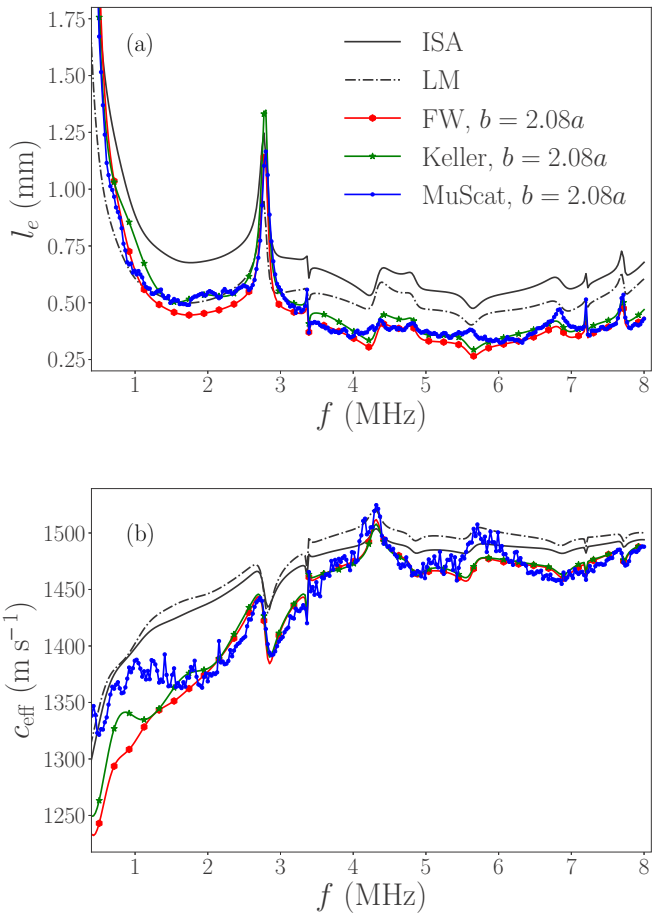

FIG. 7. Scattering mean-free path (a) and effective phase velocity (b) calculated with MuScat (diamonds markers), Keller, FW, ISA, and LM models for concentration $\phi = 60\%$. Frequency range corresponds to $ka \in [1.0\text{–}13.4]$.

results for such high concentrations. It is probably due to the fact that, around this specific frequency, the coherent wave is strengthened by the resonance. It may be argued that scatterers store the energy at resonant frequencies (in the steady state), which, in effect, reduces the intensity of interactions between cylinders (because there is less energy traveling in the ambient fluid) and could explain why the decrease of the attenuation related to the multiple scattering becomes less sensitive to the concentration. Out of resonance frequencies, Keller and FW models as well as MuScat give results that get away significantly from ISA and LM predictions especially as the concentration increases. This result is consistent with what is known about the role of the concentration. We can also note the presence of oscillations on the effective phase velocity with MuScat that appear visibly smoother with FW and Keller models but which are not observed with ISA and LM models. Once again, this can seen as the sign of the influence of the microstructure.

C. Correlation effects at concentration $\phi = 60\%$

In order to enhance our analysis, we have investigated the propagation of coherent waves in a highly concentrated medium, $\phi = 60\%$, over a large frequency range, between $f = 0.6$ MHz and $f = 8$ MHz, which corresponds to ka ranging from 1.0 to 13.4 [see Figs. 7(a) and 7(b)]. Conclusions remain the same. The degree of correlation b plays an important role on propagation in the small wavelength regime ($f > 2$ MHz), especially since the concentration increases. Taking into account b leads to a very good agreement between MuScat and the FW and Keller models, which reinforces the fact that the correlation is correctly introduced in the two different statistical approaches by choosing b appropriately. Imposing an exclusion distance b for these frequency regimes plays a role of "densification" of the medium, increasing the effective attenuation α_{eff} (and thus decreasing the scattering mean-free path l_e). But another regime is visible in Fig. 7, for $f < 1$ MHz, which is the opposite: for these low frequencies, increasing b increases l_e, if referring to the LM model. The next section is dedicated to the study of this regime.

Before switching to low frequencies, we just want to put a spotlight on a very interesting and amazing result of this section, namely, the very good agreement between the two homogenization models and numerical calculations, provided the correlation is taken into account. Indeed, if we compile the results of all studies about the range of validity of homogenization models in multiple scattering, with regard to the concentration, it is commonly accepted that $\phi \approx 30\%$ is the maximum acceptable value for these theories. More specifically, this maximum value is usually reached for red blood cells [43], concrete [44], or nanoparticles and colloidal dispersions [3], that is to say, for "weak" scatterers. Here cylinders are not weak, they are strongly resonant, the frequency is high, and the concentration is twice greater than 30%, which is what makes the result so surprising and interesting in itself.

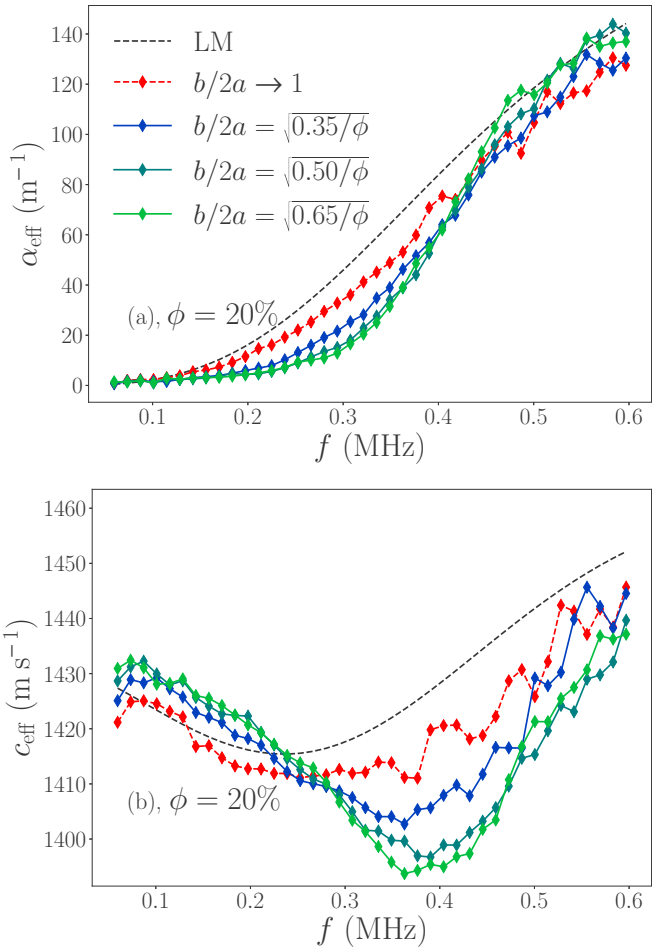

FIG. 8. Effective attenuation and phase velocity as a function of the frequency for a concentration of $\phi = 20\%$ and various values of b. Frequency range corresponds to $ka \in [0.1\text{–}1.0]$.

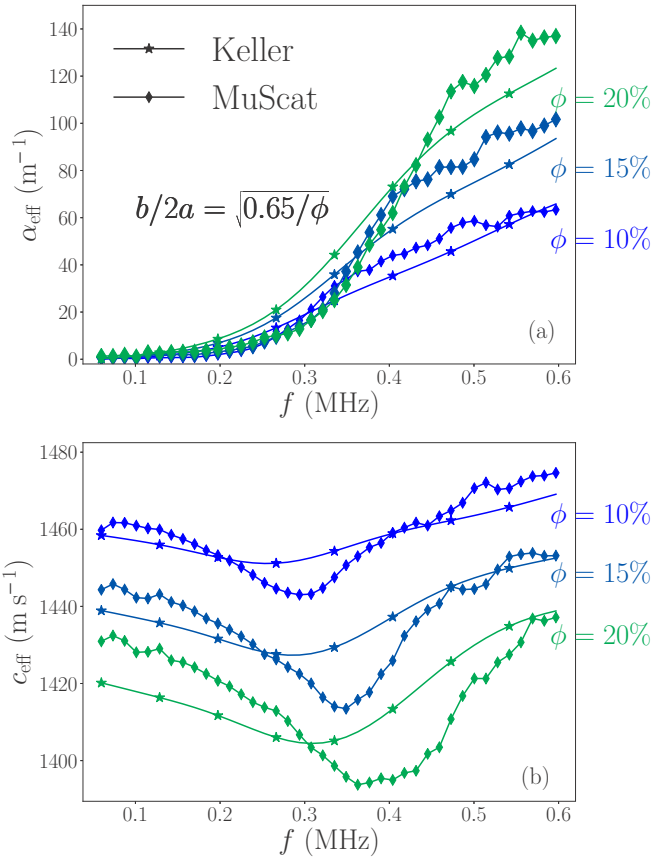

FIG. 9. Effective attenuation and phase velocity as a function of the frequency for $b/2a = \sqrt{0.65/\phi}$ and various concentrations. Frequency range corresponds to $ka \in [0.1\text{–}1.0]$.

D. Correlation effects at low frequency

This section is dedicated to understanding the predictions of the different models for $ka < 1$ ($f < 0.6$ MHz). In this regime, only few modes of vibration are sufficient to describe the propagation in the medium. As a conclusion of the last section, it has been pointed out that exclusion distance effects at low frequencies seem to be the opposite of the densification observed at high frequencies. It is not explained, but in order to go a little further into this investigation and to observe if this behavior depends on the strength of the correlation, the first step is to analyze the impact of a growing configurational constraint, keeping the concentration constant and increasing b. Doing so, we change the way in which the medium is constrained. Here, when b increases, the medium becomes more and more organized. Figures 8(a) and 8(b) give effective parameters for four different values of b [from $b/2a \to 1$ to $b/2a = \sqrt{0.65/\phi}$ as given by Eq. (17)]. Taking the case $b \to 2a$ as a reference, a transition is detected for f between 0.4 and 0.5 MHz (ka between 0.66 and 0.83). Before this window, the larger b is, the lower the effective attenuation is, whereas after this window, the larger the b is, the bigger the effective attenuation is. The influence of the correlation can also be seen on the effective phase velocity for a frequency range between 0.3 and 0.5 MHz. There is a growing gap between the velocities as b increases with a minimum around $f = 0.4$ MHz. No matter the value of b chosen, the transition always appears in the same frequency window. This study leads to two first conclusions: at low frequency range, increasing the correlation b makes the medium more transparent, and the transition between the low- and high-frequency regimes seems independent of the intensity of the configurational constraint (value of b) imposed on the microstructure. It might also be noted that MuScat and the LM model display notable differences even when $b \to 2a$, indicating that cylinders cannot be fully considered as point scatterers at these low frequencies (remember that $b \to 0$ for the LM model).

Now that we have seen the influence of the correlation, let us look at the effect of the concentration. To this end, we set b at the value given by Eq. (17), and we choose to vary ϕ between 10% and 20%. We show in Fig. 9 the Keller model that takes into account the correlation, but not the FW model, which gives nonphysical results at very low frequency with the increase of the concentration, as already noted in Refs. [44,45]. On this figure, the prevailing phenomenon is observed for $f < 0.2$ MHz ($ka < 0.3$): no matter the concentration, the attenuation seems to stay very close to zero. Increasing the concentration does not increase the attenuation in this frequency range. Here we can note that MuScat and

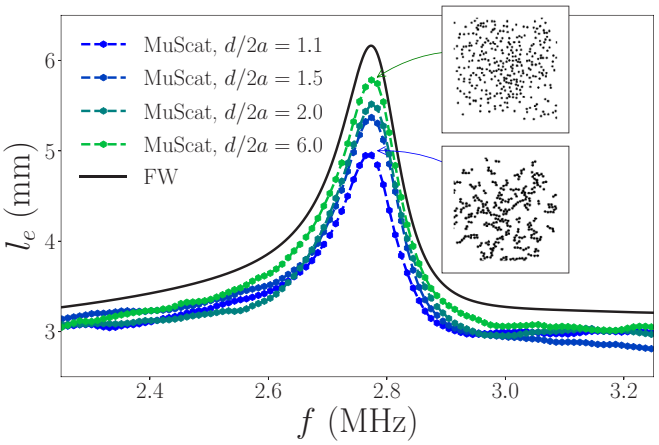

FIG. 10. Scattering mean-free path for heterogeneous media with different cluster types, with a concentration of $\phi = 10\%$. Frequency range corresponds to $ka \in [3.77–5.44]$.

Keller model display differences even at very low frequency, and, as previously observed in Fig. 8(b), there is a growing gap between the velocities for a frequency range between 0.3 and 0.5 MHz.

If we put together the results of this section with those of the previous ones, we can identify three different frequency ranges. At very low frequency, $ka < 0.3$, increasing the correlation makes the medium more transparent regardless of the concentration. In the intermediate frequency range, $0.3 < ka < 0.5$ in our case, a change of behavior is observed in the attenuation of waves, which corresponds to a situation where MuScat disagrees with statistical models by showing more complex behaviors. At high frequency, the wave attenuation increases with the increase of correlation and MuScat agrees very well with FW and Keller models up to 60% in concentration.

VI. PROPAGATION IN NONUNIFORM RANDOM MEDIA

A. Random media with clustered aggregates

To go further into the analysis of the impact of the microstructure in general, we study now two other types of constraints. The design method can be found in Sec. III B. The impact of this microstructure is quantified through the same procedure as before in order to calculate the effective parameters l_e and c_{eff}. The first is similar to the one presented in Fig. 2(a). Figure 10 shows the scattering mean-free path for four different media with the same concentration $\phi = 10\%$, constructed with four different step lengths: increasing the step length in the design procedure decreases the clustering effect. The most important phenomenon appears clearly around the resonance frequency: the shorter the step is, the weaker the resonance is. This shows that the clustering effect has a stronger impact on the resonance than the modification of the spatial organization analyzed in previous sections. This is the most significant result. Out of the resonance frequency, the predictions are approximately the same, and the clustering effect is rather smooth. To our knowledge, apart from experimental investigations, MuScat is the best tool to investigate

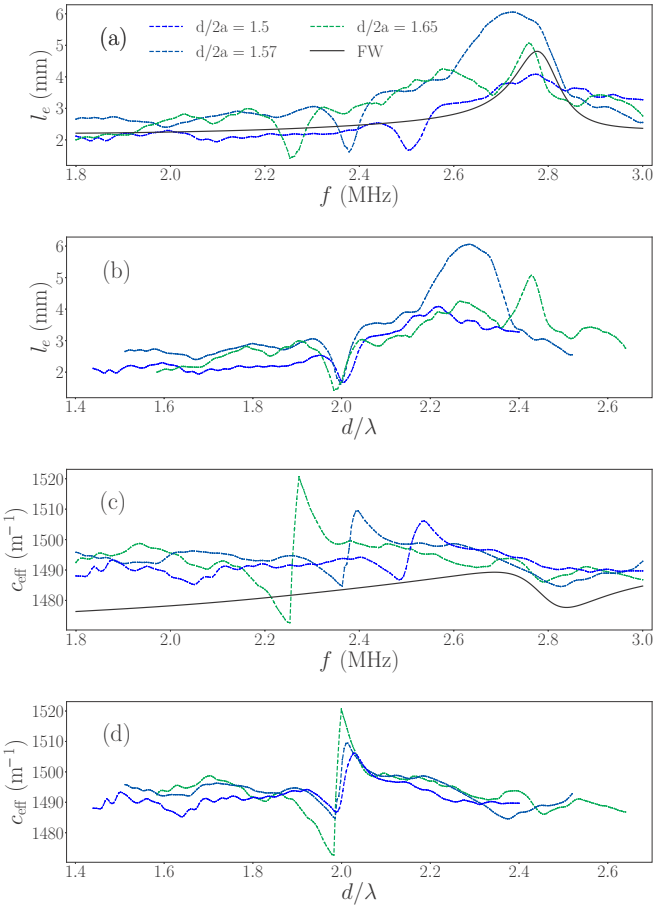

FIG. 11. Effective parameters l_e and c_{eff} of slabs with crystal-like geometrical properties (crystal with defects), such as presented in Fig. 2, plotted as a function of frequency f [(a) and (c)] and a function of d/λ [(b) and (d)]. Frequency range corresponds to $ka \in [3.0–5.0]$.

the propagation in such media, which are beyond the reach of statistical models considered in previous sections.

B. Random media with periodic aggregates

This last microstructure is the one presented in Fig. 2(b). We consider here a concentration of $\phi = 15\%$. As said in Sec. III B, the design procedure is the same as in Ref. [34]. In the case of fully crystalline solids, remember that Bragg's law that gives the maximum constructive interference condition for the waves scattered by the crystal is written as

$$2d \cos\theta_{\text{inc}} = n\lambda, \tag{18}$$

with θ_{inc} the incidence angle ($\theta_{\text{inc}} = 0$ corresponds to the normal incidence), λ the wavelength, and n a positive integer. The question we ask here is: How much is a coherent wave sensitive to the quasiperiodic organization of the random microstructure?

The numerical results calculated with MuScat are plotted in Fig. 11 as a function of frequency [Figs. 11(a) and 11(c)] and as function of d/λ [Figs. 11(b) and 11(d)]. In our case $\theta_{\text{inc}} = 0$, so that interferences may occur for $d/\lambda = n/2$ as pointed out by Eq. (18). For the frequency such that $d/\lambda = 2$

a decreasing of the scattering mean-free path l_e and a jump on the effective phase velocity c_{eff} are observed. This is the more visible phenomenon which is observed for this kind of microstructure. The resonance specific to each cylinder does not emerge clearly as before. The behavior of this microstructure is very different from the other ones.

According to the point of view, the medium can be considered as crystal with random defects, but also as a collection of small clusters, each of them containing a few periodically spaced cylinders. In line with this last interpretation, with the idea in mind that the medium is purely random, it is the resonance due to interferences inside the small periodic clusters that are observed on effective parameters.

VII. CONCLUSIONS

In this work we have addressed the question of the role of the microstructure of random heterogeneous media on the propagation of coherent waves. The first basic idea was to introduce an exclusion distance b around the particles into the models and to show that b is in direct relation to the spatial correlation and the degree of organization of the random medium. Our study leads to the conclusion that the impact of this constraint can be understood as a correlation effect. This correlation appears not to have the same influence on the propagation according to the frequency: at low frequency, increasing the configurational constraint of the samples makes the medium more transparent, whereas in the high-frequency regime, it leads to an "opacification" of the medium. At very low frequencies ($ka < 0.3$), MuScat and Keller models display differences. The numerical model shows that, no matter the concentration, the attenuation seems to stay very close to zero. Increasing the concentration does not increase the attenuation in this frequency range. As far as we know, these results are new in the literature and could not be discussed without an exact method taken here as a reference.

Surprisingly enough, Keller and FW homogenization models appear to describe very well the propagation of coherent waves at small wavelength up to very large concentrations ($\phi = 60\%$), when these models are commonly assumed to be inefficient for studying such concentrated media.

The impact of nonuniform configurational constraint has also been studied in the last part of this work, enlightening the fact that clustering has a local impact around the resonant frequency, and can also lead, when adding a periodic constraint on the random clusters, to network effects. This last conclusion leads to the idea that the propagation in heterogeneous media cannot be fully understood without a precise analysis of its microstructure.

ACKNOWLEDGMENTS

The authors would like to thank Arnaud Derode, Victor Mamou, and Arnaud Tourin (ESPCI Paris, PSL Research University, CNRS, Univ Paris Diderot, Sorbonne Paris Cité, Institut Langevin, UMR 7587) for kindly providing the data of their experimental results.

[1] R. J. Elliot, J. A. Krumhans, and P. L. Leath, Rev. Mod. Phys. **46**, 465 (1974).
[2] A. Lagendijk and B. van Tiggelen, Phys. Rep. **270**, 143 (1996).
[3] R. E. Challis, M. J. W. Povey, M. L. Mather, and A. K. Holmes, Rep. Prog. Phys. **68**, 1541 (2005).
[4] J. Mei, Z. Liu, W. Wen, and P. Sheng, Phys. Rev. B **76**, 134205 (2007).
[5] G. Haïat, A. Lhémery, F. Renaud, F. Padilla, P. Laugier, and S. Naili, J. Acoust. Soc. Am. **124**, 4047 (2008).
[6] D. Torrent and J. Sánchez-Dehesa, Phys. Rev. B **74**, 224305 (2006).
[7] V. Leroy, A. Strybulevych, J. H. Page, and M. G. Scanlon, J. Acoust. Soc. Am. **123**, 1931 (2008).
[8] O. Lesueur, R. Pierrat, and R. Carminati, Optica **3**, 763 (2016).
[9] U. Frisch, *Probabilistic Methods in Applied Mathematics*, Vol. 1 (A. T. Bharucha-Reid, New York, 1968).
[10] E. Economou, *Green's Functions in Quantum Physics*, Vol. 1 (Springer-Verlag, Berlin, 1979).
[11] S. M. Rytov, Y. A. Kravtsov, and V. I. Tatarskii, *Principles of Statistical Radiophysics*, Vol. 4 (Springer-Verlag, Berlin, 1989).
[12] P. Sheng, *Introduction to Wave Scattering, Localization and Mesoscopic Phenomena* (Academic, New York, 1995).
[13] L. Tsang and J. A. Kong, *Scattering of Electromagnetic Waves: Advanced Topics* (Wiley, New York, 1995).
[14] P. A. Martin, *Multiple Scattering: Interaction of Time-Harmonic Waves with N Obstacles* (Cambridge University Press, Cambridge, 2006).
[15] L. L. Foldy, Phys. Rev. **67**, 107 (1945).
[16] M. Lax, Phys. Rev. **85**, 621 (1952).
[17] P. C. Waterman and R. Truell, J. Math. Phys. **2**, 512 (1961).
[18] P. M. Spelt, M. A. Norato, A. S. Sangani, M. S. Greenwood, and L. L. Tavlarides, J. Fluid Mech. **430**, 51 (2001).
[19] M. Baudoin, J. L. Thomas, F. Coulouvrat, and D. Lhuillier, J. Acoust. Soc. Am. **121**, 3386 (2007).
[20] T. Valier-Brasier, J. M. Conoir, F. Coulouvrat, and J. L. Thomas, J. Acoust. Soc. Am. **138**, 2598 (2015).
[21] R.-B. Yang and A. K. Mal, J. Mech. Phys. Solids **42**, 1945 (1994).
[22] C. M. Linton and P. A. Martin, J. Acoust. Soc. Am. **6**, 3413 (2005).
[23] A. N. Norris and J. M. Conoir, J. Acoust. Soc. Am. **129**, 104 (2011).
[24] F. C. Karal and J. B. Keller, J. Math. Phys. **5**, 537 (1964).
[25] R. M. Christensen and K. H. Lo, J. Mech. Phys. Solids **27**, 315 (1979).
[26] F. J. Sabina and J. R. Willis, Wave Motion **10**, 127 (1988).
[27] S. Kanaun, V. Levin, and F. Sabina, Wave Motion **40**, 69 (2004).
[28] J. Y. Kim, J. Acoust. Soc. Am. **127**, 2201 (2010).
[29] A. L. Gower, I. D. Abrahams, and W. J. Parnell, Proc. R. Soc. A **475**, 20190344 (2019).
[30] J. F. Chaix, M. Rossat, V. Garnier, and G. Corneloup, J. Acoust. Soc. Am. **131**, 4481 (2012).
[31] A. Derode, V. Mamou, and A. Tourin, Phys. Rev. E **74**, 036606 (2006).

[32] A. Rohfritsch, J.-M. Conoir, R. Marchiano, and T. Valier-Brasier, J. Acoust. Soc. Am. **145**, 3320 (2019).
[33] G. M. Conley, M. Burresi, F. Pratesi, K. Vynck, and D. S. Wiersma, Phys. Rev. Lett. **112**, 143901 (2014).
[34] P. Mallet, C. A. Guérin, and A. Sentenac, Phys. Rev. B **72**, 014205 (2005).
[35] F. A. Amirkulova and A. N. Norris, J. Comput. Phys. **299**, 787 (2015).
[36] S. Koc and W. C. Chew, J. Acoust. Soc. Am. **103**, 721 (1998).
[37] N. A. Gumerov and R. Duraiswami, J. Acoust. Soc. Am. **11**, 1744 (2005).
[38] N. A. Gumerov and R. Duraiswami, *Fast Multipole Methods for the Helmholtz Equation in Three Dimensions* (Elsevier, 2004).
[39] J. G. Fikioris and P. C. Waterman, J. Math. Phys. **5**, 1413 (1964).
[40] W. J. Parnell and I. D. Abrahams, Wave Random Complex **20**, 678 (2010).
[41] B. A. van Tiggelen and A. Lagendijk, Phys. Rev. B **50**, 16729 (1994).
[42] M. Caleap, B. Drinkwater, and P. D. Wilcox, J. Acoust. Soc. Am. **131**, 2036 (2012).
[43] E. Franceschini, B. Lombard, and J. Piraux, J. Phys.: Conf. Ser. **269**, 012014 (2011).
[44] T. Yu, J. F. Chaix, L. Audibert, D. Komatitsch, V. Garnier, and J.-M. Hénault, Ultrasonics **92**, 21 (2019).
[45] M. Chekroun, L. Le Marrec, B. Lombard, and J. Piraux, Wave Random Complex **22**, 398 (2012).